Transition of the Large-Scale Atmospheric and Land Surface Conditions from the Dry to the Wet Season over Amazonia as Diagnosed by the ECMWF Re-Analysis

WENHONG LI AND RONG FU

Earth and Atmospheric Sciences, Georgia Institute of Technology, Atlanta, Georgia

(Manuscript received 21 November 2002, in final form 29 December 2003)

ABSTRACT

Using 15-yr instantaneous European Centre for Medium-Range Weather Forecasts Re-Analysis (ERA) data, the authors have examined the large-scale atmospheric conditions and the local surface fluxes through the transition periods from the dry to wet seasons over the southern Amazon region (5°–15°S, 45°–75°W). The composite results suggest that the transition can be divided into three phases: initiating, developing, and mature. The initiating phase is dominated by the local buildup of the available potential energy. This begins about 90 days prior to the onset of the wet season by the increase of local land surface fluxes, especially latent heat flux, which increases the available potential energy of the lower troposphere. The cross-equatorial flow and upper-tropospheric circulation remain unchanged from those of the dry season. The developing phase is dominated by the seasonal transition of the large-scale circulation, which accelerates by dynamic feedbacks to an increase of locally thermal-driven rainfall, starting about 45 days before the onset of the wet season. During this stage, the reversal of the low-level, cross-equatorial flow in the western Amazon increases moisture transport from the tropical Atlantic Ocean and leads to net moisture convergence in the southern Amazon region. In the upper troposphere, the divergent kinetic energy begins to be converted into rotational kinetic energy, and geopotential height increases rapidly. These processes lead to the onset of the wet season and the increase of anticyclonic vorticity at the upper troposphere. After onset, the lower-tropospheric potential energy reaches equilibrium, but the conversion from divergent to rotational kinetic energy continues to spin up the upper-tropospheric anticyclonic circulation associated with the Bolivian high until it reaches its full strength.

This analysis suggests that a weaker (stronger) increase of land surface latent (sensible) heat flux during the dry season and the initiating phase tends to delay the large-scale circulation transition over the Amazon. The influence of land surface heat fluxes becomes secondary during the developing and mature phases after the transition of the large-scale circulation begins. A later northerly reversal and/or weaker cross-equatorial flow, a later southerly withdrawal of the upper-tropospheric westerly wind, and a stronger subsidence could delay and prolong the developing phase of the transition and consequently delay the onset of the Amazon wet season.

1. Introduction

The wet-season onset date and the amount of rainfall are critical for agriculture, hydroelectric power generation, and local ecosystems of the Amazon region. Liebmann and Marengo (2001) have shown that a change in the timing of onset and the end of the rainy season contributes more to the interannual variation of precipitation than does a change of the intensity of precipitation during the rainy season. However, what controls the timing of the onset and its variability over South America is still unclear. In particular, it is not known how the local land surface flux increase and the land–ocean surface temperature gradient contribute to the destabilization of the atmosphere and the increase of water vapor needed for wet-season rainfall. The answer to this question is key for understanding the interannual variability of the precipitation and for determining the climatic impact of land use in the region. For example, if the land surface latent heat flux is an important source of moisture for the transition, a preseasonal decrease in the surface latent heat flux would effectively slow the transition and delay the onset of the wet season. On the other hand, if the primary source of moisture is the transport from the Atlantic, a preseasonal dry condition would enhance the moisture transport from the Atlantic Ocean, as a result of a stronger surface sensible heat flux and consequently a stronger land–ocean temperature gradient. This preseasonal dry condition would accelerate, instead of decelerate, the transition from dry to wet seasons.

Whether the local land surface fluxes or remote influences from adjacent oceans control the rainfall and circulation of the wet season has been debated for years. For example, Gutman and Schwerdtfeger (1965), Salati et al. (1979), and Rao and Erdogan (1989) suggested that the land surface fluxes control the wet-season cir-

Corresponding author address: Dr. Rong Fu, Earth and Atmospheric Sciences, Georgia Institute of Technology, Ford ES&T Bldg., 311 Ferst Dr., Atlanta, GA 30332-0340.
E-mail: fu@eas.gatech.edu

culation pattern over South America and are main contributors of moisture in the wet season. On the other hand, many other studies (e.g., Namias 1972; Serra 1973; Rowntree 1976; Hastenrath and Heller 1977; Markham and McLain 1977; Covey and Hastenrath 1978; Moura and Shukla 1981; Aceituno 1988; Ropelewski and Halpert 1989; Fu et al. 2001) have suggested that the sea surface temperatures (SSTs) in the tropical Atlantic and Pacific Oceans strongly control the precipitation over the Amazon through the direct thermal circulation of the Atlantic intertropical convergence zone (ITCZ), as well as by Rossby waves propagating from the extratropical South Pacific to subtropical South America. According to these studies, the main source of moisture during the wet season is the transport from the Atlantic (e.g., Gibbs 1979; Rao et al. 1996). How to reconcile the apparent differences obtained by these two groups of researchers as to the role of land versus ocean in initiating the monsoon has been unclear.

Fu et al. (1999) examined how the atmosphere is destabilized during the transition from dry to wet seasons. They observed that a moistening planetary boundary layer (PBL) and a weakened inversion due to declining temperatures at the top of the PBL appear to be the main contributors to the destabilization. Their results suggest that half of the extra moisture in the PBL during the wet season is obtained from the entrainment of more humid air during diurnal growth of the PBL. Moisture transport that increases the humidity above the PBL is thus an important contributor to the moisture increase in the PBL. These results were obtained by comparing a dry season with a peak wet season, although whether they are applicable to the transition period was not established.

The importance of the large-scale dynamical processes to the onset of the rainy season has been suggested by many previous studies. However, most such earlier studies have focused on the relationships among Amazon convection, the Bolivian high, and large-scale, lower-level flow during the peak phase of the Amazon rainy season (e.g., Virji 1981; Nishizawa and Tanaka 1983; Chu 1985; Hastenrath 1990). Whether such relationships characterize the expected dynamic responses to tropical convection (Gill 1980) or the causes of the convection has been unclear. Horel et al. (1989) have suggested that deep convection in the Amazon basin appeared prior to the establishment of the Bolivian high in the case of 1985–86. This implies that the Bolivian high may be a result, instead of a cause, of the Amazon precipitation. This is consistent with the numerical simulations of Silva Dias et al. (1983), Gandu and Geisler (1991), and Lenters and Cook (1997), which indicate that the latent heat released by Amazon convection is needed for building up the Bolivian high to its observed strength. Hence, the onset of the rainy season in the Amazon could be an early step in the transition to the South American summer monsoon circulation. Therefore, the processes that control the convection prior to the establishment of the Bolivian high are probably also crucial to the onset of the South American summer monsoon.

Examining how the increased solar energy is transformed into kinetic energy to support the development of the wet-season circulation can also shed light on the dynamic processes that drive the transition. Krishnamurti et al. (1998) examined the mature south Asian monsoon system and found that the increased available potential energy (APE) provided by differential heating between land and ocean is sufficient to support the summer south Asian monsoon circulation. Such APE is first converted into divergent kinetic energy and then transformed into rotational kinetic energy.[1] The latter spins up the upper tropospheric anticyclonic flow. Moscati and Rao (2001) have applied a similar analysis of energy conversion to the mature South American monsoon system. They found that APE is converted into divergent kinetic energy through a direct circulation response to the atmospheric heating. The conversion from divergent to rotational kinetic energy is similar to that of the south Asian monsoon. In this study, instead of examining a mature monsoon system, we will examine the energy conversions during the transitions from dry to wet seasons by using instantaneous European Centre for Medium-Range Weather Forecasts (ECMWF) Re-Analysis (ERA) data and the formulas of Krishnamurti and Ramanathan (1982) and Krishnamurti et al. (1998). This study provides a systematic assessment of the processes that initiate and accelerate the transition to the wet-season onset over the southern Amazon region and may also help to identify potential predictors. In the next section, data and primary methods are described and the definition of the onset of the wet season is also discussed. Section 3 gives the results. The discussion and conclusions are given in the last two sections.

2. Data and methods

a. Datasets

We use ERA, rain gauge data (Liebmann and Marengo 2001; Marengo et al. 2001), and the Global Precipitation Climatology Project (GPCP) blended precipitation data in this study. The rain gauges are located within the Brazilian Amazon basin and the rain gauge precipitation data were originally obtained from the National Water and Electric Energy Agency of Brazil [Agência Nacional de Energia Elétrica (ANEEL)]. ERA has produced global reanalysis 4 times daily from 1979 to 1993. To determine how well ERA precipitation data

[1] The APE is proportional to $1/V \int \theta'^2/\theta^2\, dV$, where V is the total volume, θ is the average potential temperature for a given pressure surface over the chosen spatial domain, and θ' is the local deviation from the average. The divergent and rotational kinetic energy are defined as $(1/2)[(-\partial\chi/\partial x)^2 + (-\partial\chi/\partial y)^2]$ and $(1/2)[(-\partial\psi/\partial y)^2 + (\partial\psi/\partial x)^2]$, respectively, where χ and ψ are velocity potential and streamfunction.

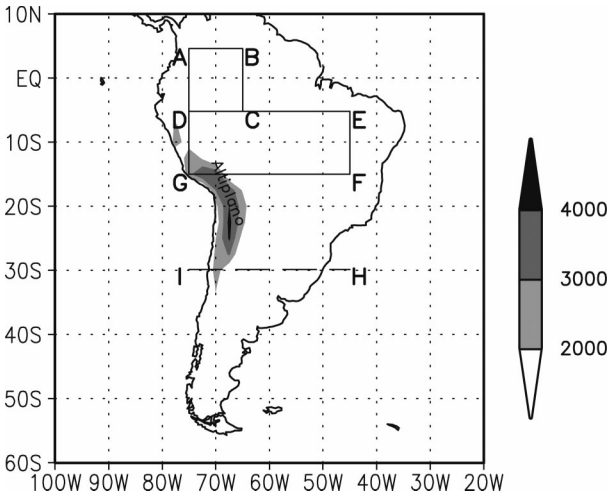

FIG. 1. The domains for the V index (5°S–5°N, 65°–75°W, ABCD), southern Amazon region (5°–15°S, 45°–75°W, DEFG), and the extension for geopotential height at 200 hPa $Z_{200\,\mathrm{hPa}}$ (5°–30°S, HI), respectively. The darkest shaded region indicates terrain elevation in excess of 4000 m.

represent the rainfall pattern in the Amazon basin, these data at 2.5° latitude × 2.5° longitude resolution were compared to the rain gauge data and GPCP data in the domain of 5°–15°S, 45°–75°W (Fig. 1, domain DEFG, referred to hereafter as the southern Amazon region) for the same period. The most significant discrepancy between the datasets is that ERA overestimates dry-season rainfall by as much as 3 mm day^{-1} compared to rain gauge measurements (Fig. 2a). During the wet season, ERA data are comparable to those of GPCP. ERA rainfall is about 2–3 mm day^{-1} lower than that of rain gauge data. The assimilated seasonal cycle of rainfall is evaluated by removing the climatological annual mean calculated for the period 1979–93 (Fig. 2b). The timing and general trends of the transition from the dry to the wet seasons derived from ERA are similar to those of rain gauge and GPCP data, although the rate of increase is only about half that of observations. The calendar date of rain-rate increase during the early stage of the transition obtained from ERA is delayed by nearly 10 days, compared to that of the rain gauge data. To address the impact of the error in the ERA rain rate, we will use the observed rain rates as well as those of ERA in our composite analysis.

Very few other observations of atmospheric and surface conditions related to rainfall over the Amazon are available. Fu et al. (2001) compared the climatological monthly mean vertical profiles of temperature, humidity, and zonal and meridional winds assimilated by ERA with those derived from radiosondes at Manaus, Brazil, (3°S, 60°W) for each calendar month during the period 1987–93. Their comparison (their Figs. 5 and 6) sug-

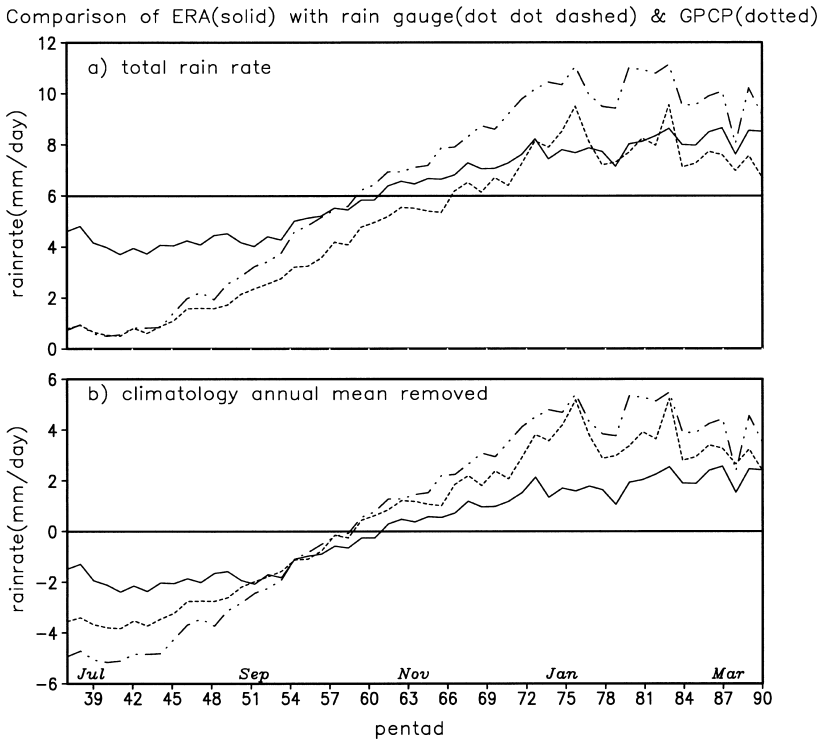

FIG. 2. (a) The 15-yr (1979–93) mean seasonal variations of pentad rain rate (mm day^{-1}) for ERA (solid line), GPCP (dotted line), and rain gauge data from ANEEL (dot–dot–dashed line) averaged over the southern Amazon region; (b) same as (a), but the climatology annual mean has been removed.

gests a less than 1-K difference in temperature profiles, a good agreement of humidity between 925 and 100 hPa, and less than 10% systematically overestimated humidity between the surface and 925 hPa, which probably causes about a 1 kJ kg^{-1} systematic increase of convective available potential energy (CAPE) and decrease of convective inhibition energy (CINE). The differences of zonal and meridional wind profiles were less than 2 m s^{-1} below 200 hPa. Betts and Jakob (2002) have carefully compared the surface fluxes and structure of the PBL of the current ECMWF short-term forecast model with in situ observations from the Wet-Season Atmospheric Mesoscale Campaign (WETAMC) of the Large-scale Biosphere–Atmosphere Experiment in Amazonia (LBA). They found that the model biases were rather small for the mean diurnal cycles of potential temperature, mixing ratio, equivalent potential temperature, and the pressure height of the lifting condensation level. The ECMWF model was also able to qualitatively capture the patterns and relative importance of each type of flux in the surface energy budget equation for the wet-season condition, but quantitatively tended to overestimate the net radiative flux by as much as 10%. This extra incoming energy was largely balanced by a greater latent heat flux. The model that Betts and Jakob (2002) examined uses a new land surface model; therefore, the simulated surface fluxes may differ from those of ERA.

A smoothing procedure was used by ECMWF to compensate for the drying of land surface soils caused by the inadequate land surface model in ERA. This approach provides land surface fluxes consistent with the surface air humidity, but does not conserve water. To evaluate how well ERA can represent the changes of surface sensible and latent heat fluxes during the transition from the dry to wet seasons, we compare their assimilated values to the in situ observations from the Anglo-Brazilian Climate Observation Study (ABRACOS) sites in Reserva Jaru (10°05′S, 61°55′W; near Ji-Parana, Rondonia) and Reserva Vale (5°45′S, 49°10′W; near Maraba, Para) during the transition period from the dry to wet seasons in 1992 and 1993. Given the spatial-scale difference between ERA and the in situ measurements from the ABRACOS flux towers, complete agreement should not be expected. Figure 3 shows the comparisons of the surface fluxes between ERA and the observations. Despite lower biases in latent and sensible heat fluxes of ERA during the dry season (pentads 19–41, where a pentad is a 5-day period), the trends of both fluxes are consistent with those observed. During the early transition period (pentads 45–51) when, as we will show later, the surface fluxes are most critical to the transition, the latent heat flux agrees with the observations in both trend and magnitude. During the developing phase (pentads 51–60), the surface latent heat flux in ERA data ceases to increase at pentad 53, about 20 days earlier than the time observed by ABRACOS, leading to about a 30–40 W m^{-2} (20%–25%) underestimate of surface latent heat flux in ERA in early October. The maximum discrepancies occurred during the developing phase when the large-scale circulation changes dominate the increase of rainfall; thus, the aforementioned discrepancies probably will not change the main character of the transition. Figure 3 suggests that ERA data are able to qualitatively assimilate the trend of surface latent heat fluxes during the early transition from the dry to wet seasons in 1992 and 1993, despite ERA problems with the treatments of soil moisture and other land surface parameters. In short, ERA appears to reasonably capture the evolution of atmospheric circulation and land surface fluxes key to the transition from the dry to wet seasons over the Amazon.

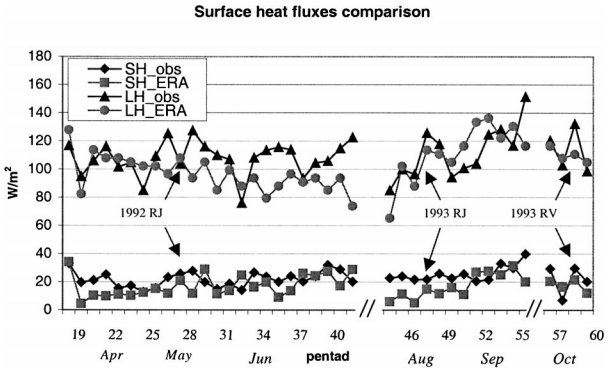

FIG. 3. Time series of the surface sensible heat (SH) and latent heat (LH) fluxes averaged over 1992 and 1993. The surface fluxes obtained from ERA are plotted in curves with squares (SH) and dots (LH), respectively. The surface fluxes obtained from in situ ABRACOS observations are plotted in curves with diamonds (SH) and triangles (LH), respectively. The numbers of pentads in the abscissa are determined by their calendar dates. The ABRACOS observations of SH and LH are obtained from the tower measurements at the forest site in Reserva Jaru (RJ; 10°05′S, 61°55′W) near Ji-Parana, Rondonia, and Reserva Vale (RV; 5°45′S, 49°10′W) near Maraba, Para. The ERA SH and LH are obtained from the 2.5° grid box overlap with the ABRACOS sites. The unit is W m^{-2}.

We use horizontal wind, vertical velocity, geopotential height, temperature, relative humidity, and specific humidity from ERA data at 13 levels (1000, 925, 850, 775, 700, 600, 500, 400, 300, 250, 200, 150, and 100 hPa, respectively) to derive the atmospheric thermal and dynamic fields related to the change of rainfall for the southern Amazon region. All variables in the study, especially those nonlinear terms related to the input fields, are first computed from instantaneous input values at 6-h intervals. They are then averaged over a pentad. The pentad resolution has been shown to minimize daily variations and noise, while remaining fine enough to resolve the changes during the transition from the dry to wet seasons over the Amazon (e.g., Kousky 1988; Horel et al. 1989).

b. Domain of the analysis

Because the peak of the rainy season varies from July in the northern Amazon to January in the southern Am-

azon, we restrict the domain to the southern Amazon region (5°–15°S, 45°–75°W) to more clearly capture the seasonal cycle of rainfall over the Southern Hemisphere Amazon. This domain is mostly within the Amazon basin, except for the inclusion of a small segment of the Andes in the southwestern corner of the domain. As shown in Kousky (1988) and Marengo et al. (2001), the wet-season onset in this domain generally occurs in austral spring, before the establishment of the South American summer monsoon. The increase of rainfall after the wet-season onset in this domain presumably provides the needed latent heat for the development of the Bolivian high (Silva Dias et al. 1983; Gandu and Geisler 1991; Lenters and Cook 1997). Because the upper-tropospheric high is expected to occur to the southwest of the latent heating in the Amazon (e.g., Gill 1980; Lenters and Cook 1997), we expand the southern boundary of our domain southward to 30°S for diagnosing the changes of 200-hPa geopotential height (Fig. 1, dashed line HI). This expansion allows a more complete inclusion of the upper-tropospheric response to the Amazon heating and the Bolivian high.

c. Computation of the key variables

One effective way to understand what drives the transition from the dry to wet seasons over South America is to clarify the similarities and differences between the South American and the more thoroughly studied south Asian monsoon system. Specifically, we aim to clarify whether the circulation of the wet season over the southern Amazon region is driven by similar atmospheric dynamic processes. We also hope to determine whether the onset of the wet season over the Amazon is initiated mainly by an increase of the surface sensible heat flux, as occurs in the south Asian monsoon, or by an increase of the surface latent heat flux. The former leads to the reversal of the land–ocean temperature gradient and consequently to the reversal of the low-level, cross-equatorial flow and moisture transport. The area remains very dry until the reversal of the cross-equatorial flow. If the latter is the case, an increase of the surface latent heat flux could destabilize the local atmosphere and increase convection even before the reversal of the large-scale wind and moisture transport. The sensitivity of the monsoon onset to the surface fluxes would be very different in these two cases. To clarify how the onset of the wet season over the Amazon is initiated, we will examine the evolution of the lower-tropospheric moist static energy, the cross-equatorial flow that transports moisture into the domain, energy conversion, and the circulation at the upper troposphere. These conditions are represented by the equivalent potential temperature (θ_e) at 850 hPa, the V index (Wang and Fu 2002), net moisture convergence, the conversion function between the atmospheric divergent and rotational kinetic energy (C), and 200-hPa geopotential height ($Z_{200\ \mathrm{hPa}}$).

Equivalent potential temperature is computed from instantaneous temperature and specific humidity from ERA. The tendency of $\theta_e(\partial\theta_e/\partial t)$ is computed from the difference between subsequent daily mean θ_e and previous daily mean θ_e divided by the 2-day interval in units of kelvins per day. Five daily values are then averaged to obtain a pentad averaged value $\partial\theta_e/\partial t$. To diagnose the causes of increasing $\partial\theta_e/\partial t$ at 850 hPa, we also compute the contributions of the tendencies of temperature ($\partial T/\partial t$) and specific humidity ($\partial q/\partial t$) to $\partial\theta_e/\partial t$ at 850 hPa, expressed as the following:

$$\frac{\partial\theta_e}{\partial t} \cong \underbrace{\frac{\theta_e}{T_l}\frac{\partial T}{\partial t}(1+F)}_{\mathrm{A}} + \underbrace{\frac{\theta_e}{T_l}\frac{L_c}{C_p}\frac{\partial q}{\partial t}(1-G)}_{\mathrm{B}}, \quad (1)$$

where L_c is the latent heat of vaporization, C_p is the specific heat for constant pressure, and T_l is the temperature at the lifting condensation level. Here F and G are defined:

$$F = \frac{L_c}{C_p}\frac{2840 \times 3.5q}{T_l^2(3.5\ \ln T - \ln e - 4.805)^2}, \quad (2)$$

$$G = \frac{2840 \times 0.622pq}{eT_l(3.5\ \ln T - \ln e - 4.805)^2(0.622q)^2}, \quad (3)$$

where e is the vapor pressure and p is pressure. Term A of (1) represents the contribution of $\partial T/\partial t$ to $\partial\theta_e/\partial t$ at 850 hPa, and term B represents the contribution of $\partial q/\partial t$.

CAPE and CINE are computed as in Williams and Renno (1993), then averaged over the southern Amazon region. The V index is defined as the averaged meridional wind at 925 hPa for the area of 5°N–5°S, 65°–75°W by Wang and Fu (2002; Fig. 1, domain ABCD). The net moisture convergence is calculated from the net zonal and meridional moisture transport [$\Delta(uq)$ and $\Delta(vq)$], respectively to the southern Amazon region. Zonal moisture fluxes are first integrated from 1000 to 100 hPa and from 5° to 15°S along 75° [$(uq)_{5°–15°S,\ 75°W}$] and 45°W [$(uq)_{5°–15°S,45°W}$], respectively. The net zonal moisture convergence $\Delta(uq)$ is calculated by the difference between these terms. A positive value of $\Delta(uq)$ represents a net zonal moisture convergence to the region. Similarly, $(vq)_{5°S,45°–75°W}$ and $(vq)_{15°S,45°–75°W}$ are meridional moisture fluxes integrated from 1000 to 100 hPa and along 5° and 15°S from 45° to 75°W, respectively. The net meridional moisture transport $\Delta(vq)$ is computed from the difference between these two meridional moisture transport terms. The total moisture convergence to the southern Amazon region, that is, the sum of $\Delta(uq)$ and $\Delta(vq)$, is then converted into precipitable water per day per meter squared in order to compare with the rain rate.

The energy conversion from divergent to rotational kinetic energy, C, is calculated using the formulas of Krishnamurti et al. (1998):

$$C = \langle f\nabla\psi\cdot\nabla\chi\rangle + \langle\nabla^2\psi\nabla\psi\cdot\nabla\chi\rangle + \left\langle\nabla^2\chi\frac{(\nabla\psi)^2}{2}\right\rangle + \left\langle\omega J\left(\psi, \frac{\partial\chi}{\partial p}\right)\right\rangle, \quad (4)$$

where f is the Coriolis parameter; ψ and χ are streamfunction and velocity potential, respectively; and $\langle\ \rangle$ denotes the integrations in the horizontal and vertical domain (5°–15°S, 45°–75°W, and from 1000 to 100 hPa). We calculated all the terms in formula (4), and our calculation shows that the first term $f\nabla\psi\cdot\nabla\chi$ dominates the total conversion, which agrees with the results of Krishnamurti et al. (1998) for the south Asian monsoon and of Moscati and Rao (2001) for the tropical Amazon region. This term is proportional to the projection of the divergent wind on the rotational wind. When $\nabla\psi\cdot\nabla\chi$ is negative, divergent kinetic energy transforms to rotational kinetic energy. This leads to a positive C for the negative Coriolis parameter in the Southern Hemisphere.

d. Defining the onset of the wet season

How to best define the onset of the wet season over the Amazon is still a subject of ongoing discussion (Liebmann and Marengo 2001). Kousky (1988) defined the climatological onset date by choosing a threshold of 240 W m^{-2} for the pentad outgoing longwave radiation (OLR). The onset date is identified as when OLR in 10 out of 12 subsequent pentads is below 240 W m^{-2} and OLR in 10 out of 12 previous pentads is above 240 W m^{-2}. His approach captures the large increase, both in frequency and intensity, of the precipitation associated with the onset of the wet season. His results show that the onset of the convection expands rapidly from northwest of the Amazon basin to the south and the southeast, then migrates eastward at a slower pace. Following a similar approach, Marengo et al. (2001) defined the onset of the wet season using rain gauge data in the Brazilian Amazon. They defined the onset as the time after which the rainfall exceeds 4.5 mm day^{-1} in six out of eight subsequent pentads and before which the rainfall is well below 3.5 mm day^{-1} in six out of eight preceding pentads. Their definition produces an onset pattern similar to that of Kousky (1988). However, they have also shown that the onset dates vary with the rain-rate threshold, which is somewhat arbitrary. How to objectively choose a rain-rate threshold for the onset is unclear. To address this issue, Liebmann and Marengo (2001) used the annual averaged daily rainfall of each year for each location as the threshold for the onset of that year. While such a definition objectively determines the rain-rate threshold, it leads to a very different onset pattern from those of Kousky (1988) and Marengo et al. (2001).

Our purpose is to investigate how large-scale circulation changes during the transition, rather than to determine the precise date of the onset. Nevertheless, we still need to identify a reasonable rain-rate threshold and to show that our results are qualitatively insensitive to it, as long as it is within the range of the observed annual mean rain rate over that region for the period of our analysis.

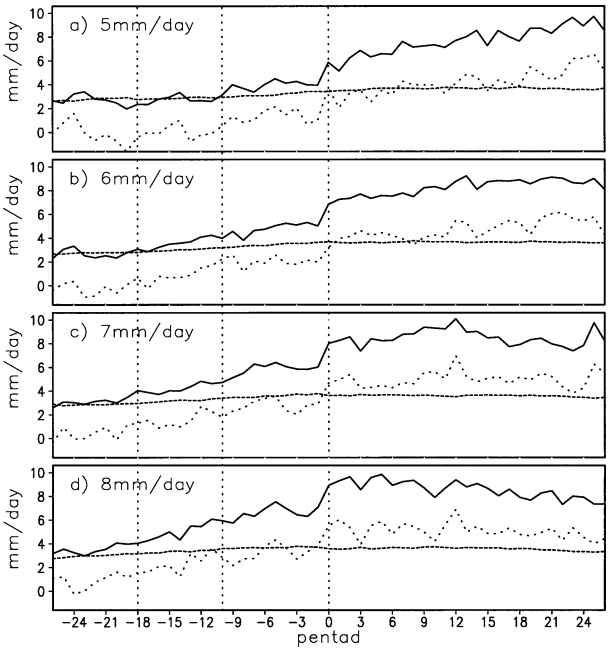

FIG. 4. Seasonal changes of the precipitation rate (mm day^{-1}; solid lines), surface evapotranspiration (mm day^{-1}; dashed lines), and net moisture convergence (dotted lines) during the transition based on different onset criteria: (a) 5, (b) 6, (c) 7, and (d) 8 mm day^{-1}.

The influence of the criteria for defining the onset on our results is examined in Fig. 4. It shows the changes of rainfall, moisture convergence, and evapotranspiration through the transition as derived from rain-rate thresholds varying from 5 to 8 mm day^{-1} of ERA, within the range of the year-to-year variation of the annual mean rain rate during the 15-yr period for the southern Amazon region. We use evapotranspiration with the unit of millimeters per day, instead of surface latent heat flux, to compare with moisture transport and rain rate. The persistent increase of rainfall and moisture convergence during the transition, the peak values, and the large increase of these two fields associated with onset are consistent among all four rain-rate thresholds tested here. The relative contributions of the evapotranspiration and moisture convergence as sources of the moisture for rainfall during the periods are also consistent among all cases. The timing of the peak rainfall and moisture convergence after the onset shifts forward relative to the onset pentad as the rainfall threshold exceeds 7 mm day^{-1}. This shift is due to the postponement of the onset date toward the peak rainy season as the onset threshold approaches the climatological seasonal peak rain rate for the southern Amazon region (8–9 mm day^{-1}).

TABLE 1. Onset dates as defined by the rain-rate threshold of 6.1 mm day^{-1}.

Year	Onset pentad	Calendar date	Annual mean rain rate (mm day^{-1})
1979	49	29 Aug–2 Sep	8.2
1980	57	8–12 Oct	6.9
1981	59	18–22 Oct	7.5
1982	68	2–6 Dec	6.0
1983	60	23–27 Oct	6.4
1984	73	26–31 Dec	4.9
1985	61	28 Oct–1 Nov	6.0
1986	73	26–31 Dec	5.7
1987	64	12–16 Nov	5.4
1988	63	7–11 Nov	5.6
1989	63	7–11 Nov	6.4
1990	60	23–27 Oct	5.9
1991	62	2–6 Nov	6.0
1992	66	22–26 Nov	4.5
1993	60	23–27 Oct	6.0

One way to objectively specify the rain-rate threshold is to use the climatological annual mean rain rate. For the southern Amazon region, the 15-yr climatology mean rain rate derived from ERA is about 6.1 mm day^{-1}. Therefore, we define the onset as the pentad before which the rain rate is less than 6.1mm day^{-1} for 6 out of 8 preceding pentads and after which the rain rate is greater than 6.1 mm day^{-1} for 6 out of 8 subsequent pentads. This definition adopts the approach of Kousky (1988) and Marengo et al. (2001) and also uses an objectively defined rain-rate threshold, as did Liebmann and Marengo (2001). The onset pentad defined by this criterion for the 15 yr is listed in Table 1.

Table 1 shows that the onset dates for the southern Amazon region vary from the end of August to December over the 15 yr. Most of the onsets occurred in October and November (11 out of 15 yr), which is generally consistent with those suggested in the literature (e.g., Satyamurty et al. 1998). The earliest onset occurred from the end of August to the beginning of September in 1979. The annual mean precipitation for this year was 8.2 mm day^{-1}, the highest in the 15-yr period. The onsets occurred at the end of December in 1984 and 1986, about 60 days later than the average onset date. The annual rain rates during these two years are lower than the climatology. This is qualitatively consistent with the relationship between the onset dates and the interannual changes of the annual precipitation found by Liebmann and Marengo (2001).

e. Composite analysis

We use the composite method to highlight the common features for the 15 transitions. Because the year-to-year variation of the onset date over the Amazon can vary by as much as three calendar months (cf. Marengo et al. 2001; also see Table 1), our composite is centered at the pentad of the onset (defined as pentad 0) of each year, rather than by calendar dates. The *n*th pentad before the onset in each year is defined as pentad *n*, and the *n*th pentad after the onset is defined as pentad *n*. Each of the composite variables for a given pentad, *i*, is calculated from the 15 values of that variable for the pentad *i* of each year during the period 1979–93. This approach enables us to more clearly focus on the large-scale circulation change associated with the evolution of the onset process, instead of on calendar dates, over the southern Amazon region.

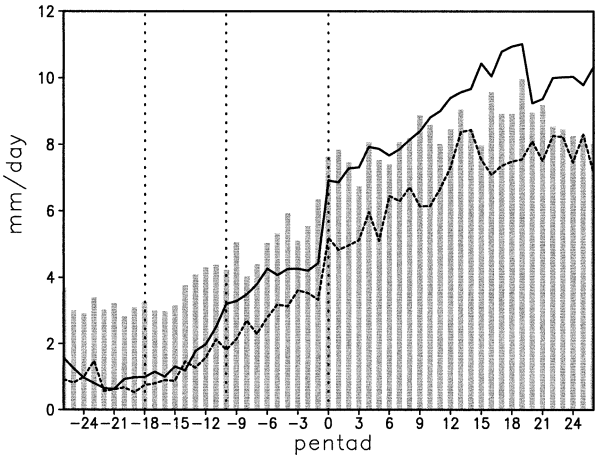

FIG. 5. Composite time series of precipitation (mm day^{-1}) for ERA (bar), GPCP (dashed line), and rain gauge data (solid line) averaged over the southern Amazon region. The three vertical dotted lines represent the beginning of the initiating, developing, and maturing phases, respectively, during the transition.

Figure 5 compares the composite evolutions of rainfall obtained from ERA with those obtained from the rain gauges and GPCP-blended precipitation data, respectively. The composite results of the rain gauges and GPCP data are calculated using the same method described above, except the onset criteria are based on their own climatological means. Figure 5 shows that the rainfall changes associated with the onset processes in ERA are more realistically assimilated than the seasonal cycle based on the calendar date, as shown in Fig. 2. This is due to the fact that our composite method allows us to remove the bias of ERA in terms of calendar onset dates and to focus on the thermal and dynamic consistency of ERA with the real transition process.

Figure 6 shows the changes of the composite variables through the transition and their corresponding 95% confidence levels using a Student's *t* distribution. The narrow confidence intervals of rain rate, V index, and moisture convergence suggest close agreement between the estimated composite values and statistically ''true'' composite values. The changes of these variables through the transition are larger than the uncertainities of the estimated values. The confidence intervals of C and $\partial\theta_e/\partial t$ are not as narrow as those of the V index, rain rate, and moisture convergence. However, C still shows statistically significant change from negative to positive from the initial phase to the onset during the

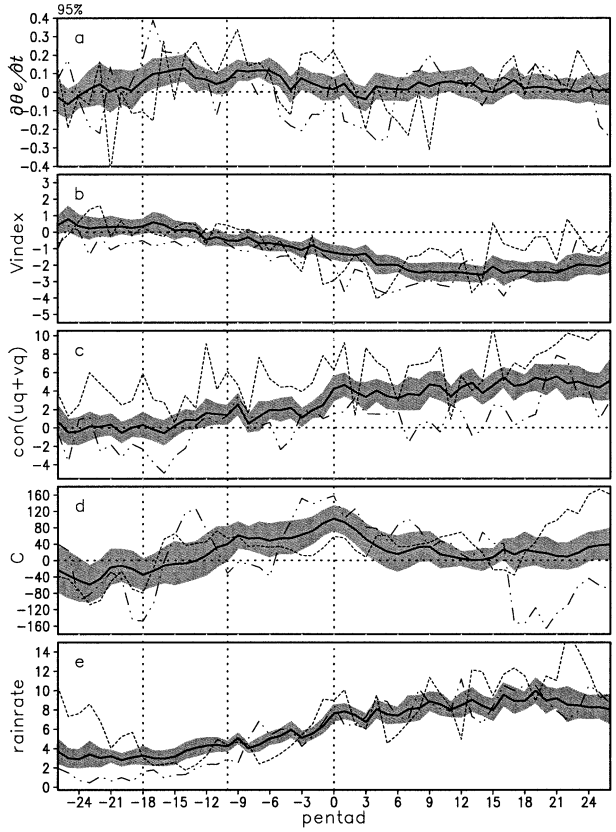

FIG. 6. Composite time series of (a) $\partial\theta_e/\partial t$ at 850 hPa (K day^{-1}), (b) the V index (m s^{-1}), (c) net moisture convergence (mm day^{-1}), (d) kinetic energy conversion function C (10^{-6} m^2 s^{-3}), and (e) rain rate (mm day^{-1}). Solid lines in (a)–(e) are the composite results for each variable. Shaded areas represent the confidence intervals at 95% significance. Dotted lines and dot–dot–dashed lines show the years with maximum positive and maximum negative departures from the composite results integrated through the entire transition periods. The three vertical dotted lines divide the times between the initiating, developing, and maturing phases, respectively, of the transition.

transition. Compared to the confidence interval, the increase of $\partial\theta_e/\partial t$ at 850 hPa is also significant for the period of pentads -18 to -4. For the rest of the transition period, especially after pentad -4, the fluctuations of $\partial\theta_e/\partial t$ at 850 hPa around zero become too small to be statistically significant. Hence, we will focus our discussion of the $\partial\theta_e/\partial t$ at 850 hPa on the early stage of the transition (from pentads -18 to -4), during which its increases are statistically significant. As we will show later, this is also the period during which the accumulation of lower-tropospheric potential energy is most critical to the transition.

The composite results are compared to extreme cases in 15 yr of the analysis. Figure 6 shows that the variables change in the years of maximum positive and maximum negative departures, respectively, from the composite results integrated through the entire transition period. Notice that the years of the extreme cases for each variable are determined independently, based on the maximum accumulated departure from its composite time series. Hence, the years of extreme cases can vary from one field to another. This approach presents a maximum possible departure of each field from its composite. As seen in Fig. 6, despite expected higher-frequency variations and systematic higher or lower shift of the curves for the extreme cases, the general trends of the V index, net moisture convergence, the energy conversion function, and rain rate for the composite and extreme cases are similar. The large deviations from the composite values for $\partial\theta_e/\partial t$ at 850 hPa from the pentads -5 to 8, and for the energy conversion function after pentad 15, suggest that the composites do not adequately represent extreme cases during these periods for these variables. Overall, Figs. 5 and 6 suggest that our composite changes are mostly statistically significant and reasonably represent the climatology of the transition.

3. Evolution of large-scale circulation and land surface conditions from the dry to wet seasons

To obtain an overall picture of the evolution of the atmospheric circulation during the transition, we examine Fig. 6 again. The time series of $\partial\theta_e/\partial t$ at 850 hPa (Fig. 6a) suggests that the increase of lower-tropospheric moist static energy starts about 90 days (18 pentads) prior to the onset date of the wet season, and such an increase diminishes soon after the onset. The lack of large-scale moisture convergence (Fig. 6c) suggests that land surface evapotranspiration must be the main contributor to the increase of moisture in the lower troposphere. Large-scale moisture convergence in the southern Amazon region and moderate increase of rainfall begins about 60 days prior to the onset (pentad -12). Ten days later, the cross-equatorial flow reverses to northerly, and the conversion from divergent to rotational energy begins (pentad -10). At or shortly after the onset, the northerly cross-equatorial, low-level flow, the net moisture convergence to the southern Amazon region, and rainfall increase rapidly. But the increase of $\partial\theta_e/\partial t$ at 850 hPa and the conversion of kinetic energy quickly diminish.

Figure 6 suggests that the transition is mainly driven by the increase of land surface fluxes, especially evapotranspiration at the beginning, but by increases of moisture transport during the developing stage and during the wet season. Three turning points can be seen during the transition; thus, we divide the transition into three phases and organize our discussion accordingly.

a. Initiating phase (pentads −18 to −10)

The initiating phase starts at 90 days and ends about 50 days prior to the wet-season onset. It is dominated by an increase of $\partial\theta_e/\partial t$ at 850 hPa (Fig. 6a), indicating a local increase of moist static energy of the lower troposphere. In the last 15 days of this phase, rainfall begins to increase, although the rate is small. Moisture

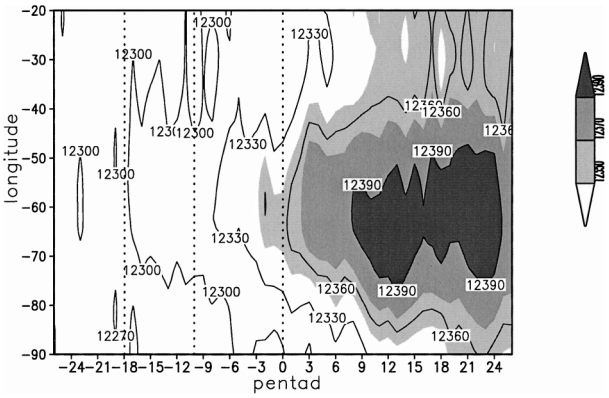

FIG. 7. Same as Fig. 5 but for composite temporal and longitudinal distribution of geopotential height at 200 hPa (m) averaged over 5°–30°S through the transition from the dry to wet seasons at pentad resolution. Contour interval is 30 m.

also begins to converge, although the low-level, cross-equatorial flow is still southerly, as in the dry season (Fig. 6b). The upper-tropospheric field remains similar to that of the dry season, as shown by the latitudinal averaged geopotential height at 200 hPa in Fig. 7. This suggests that a local θ_e at 850 hPa increases first, which thermally promotes the increase of rainfall and a lower-tropospheric moisture convergence. To diagnose the causes of increasing $\partial\theta_e/\partial t$ at 850 hPa, we examine the composite contributions of temperature and specific humidity changes [represented by terms A and B in (1) and in Fig. 8a] during 1979–93 to $\partial\theta_e/\partial t$ at 850 hPa. Before the initiating phase begins (pentad −18), the increase of temperature contributes as much as the increase of moisture to the rising $\partial\theta_e/\partial t$ at 850 hPa. During the initiating phase (pentads −18 to −10) and also through the rest of the transition period (after pentad −10), the increase of moisture becomes more important.

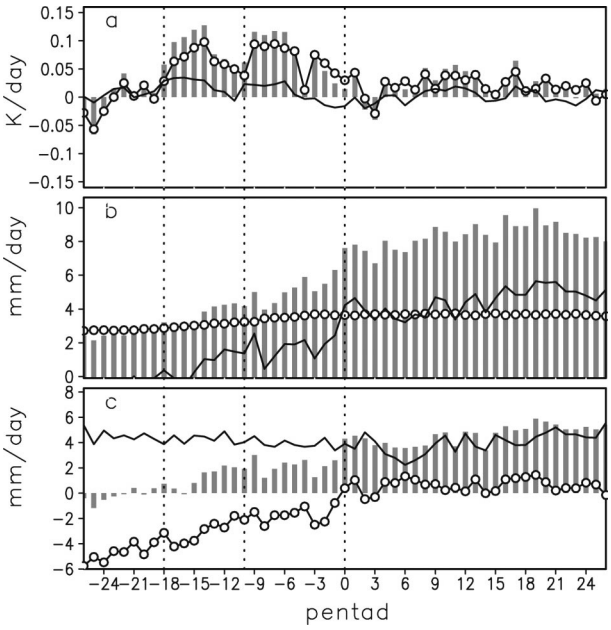

FIG. 8. Same as in Fig. 5 but for composite time series of (a) contributions of temperature change (K day^{-1}, solid line) and humidity change (K day^{-1}, solid line with circles) to $\partial\theta_e/\partial t$ at 850 hPa (K day^{-1}, bars); (b) surface evapotranspiration (mm day^{-1}, solid line with circles), net moisture convergence (mm day^{-1}, solid line), and precipitation (mm day^{-1}, bar); and (c) total moisture convergence (mm day^{-1}, bar), net zonal moisture convergence (mm day^{-1}, solid line), and net meridional moisture convergence (mm day^{-1}, solid line with circles) for the period of 1979–93 and averaged within the southern Amazon region (5°–15°S, 45°–75°W).

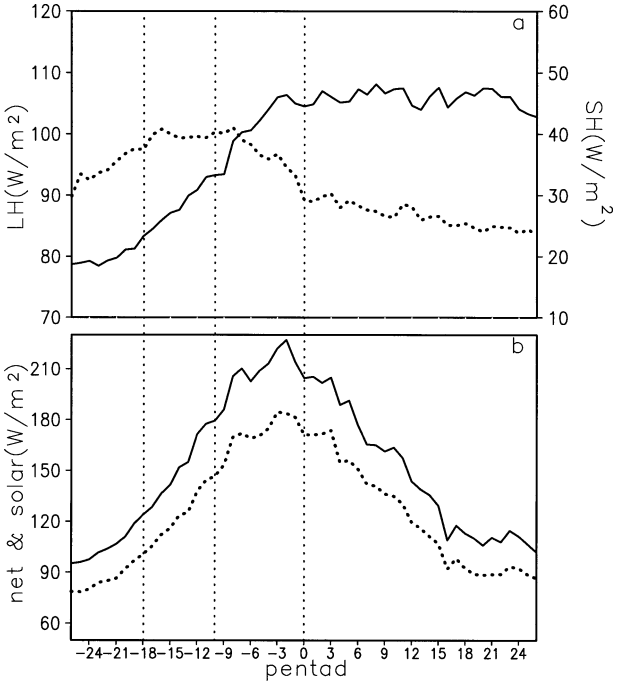

FIG. 9. Composite time series of (a) the surface LH flux (W m^{-2}; solid line, left axis) and SH flux (W m^{-2}, dotted line, right axis), and (b) downward solar radiation (W m^{-2}, solid line) and net radiation (W m^{-2}, dotted line) at the surface.

The relative importance of evapotranspiration and large-scale moisture transport during this period is illustrated in Fig. 8b, in which the net moisture convergence into the domain integrated from 1000 to 100 hPa is compared with the evapotranspiration within the region. The changes of both variables are statistically significant, although the changes of evapotranspiration appear to be smooth. During the first half of the initiating stage, when θ_e at 850 hPa begins to increase rapidly, moisture convergence is either near zero or divergent. Evapotranspiration is the main contributor to the increase of water vapor and remains the dominant source before the onset. The causes of the increase in surface evapotranspiration are examined in Fig. 9. The latent heat flux increases rapidly (Fig. 9a) with the increases of downward solar radiation and net radiation at the surface (Fig. 9b). Such an increase of the latent heat flux in response to the increase of downward solar radiation prior to the increase of rainfall is reasonable

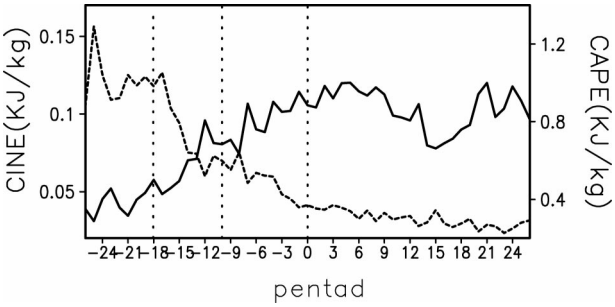

FIG. 10. Same as Fig. 5 but for CAPE (kJ kg^{-1}, solid) and CINE (kJ kg^{-1}, dotted).

based on the higher surface soil-moisture storage observed over the Amazon.

At this stage, the cross-equatorial flow in the western Amazon, as indicated by the V index, remains the same as that in the dry season. Figure 8c shows the contribution of zonal and meridional moisture transport to the net moisture convergence over the domain. The southerly cross-equatorial flow in the western Amazon (Fig. 6b) leads to a meridional divergence of moisture flux (Fig. 8c) that is strong enough to compensate for the zonal moisture convergence and cause net moisture divergence or near-zero convergence over the domain.

Figure 10 shows the variations of CINE and CAPE over the southern Amazon region. During the initiating phase, CINE decreases from 0.12 to 0.07 kJ kg^{-1}, and CAPE increases from 0.5 to about 0.7 kJ kg^{-1}. Thus, the destabilization of the atmosphere starts with the increase of surface latent heat flux 15 days prior to the moisture convergence. The evolution of the atmospheric vertical and zonal velocities, as well as of relative humidity, has been plotted along 10°S in Fig. 11. During the initiating stage, the vertical structure of the atmosphere remains similar to that of the dry season. The atmosphere above 700 hPa remains dry (RH $\leq$ 50%). Higher relative humidity (RH $\geq$ 70%) is confined to the western part of the Amazon basin. Vertical velocity is either near zero or downward over the Amazon basin. Strong westerly flow dominates at the upper troposphere (Fig. 11a). The kinetic energy conversion function is negative (Fig. 6d), indicating the absence of the diver-

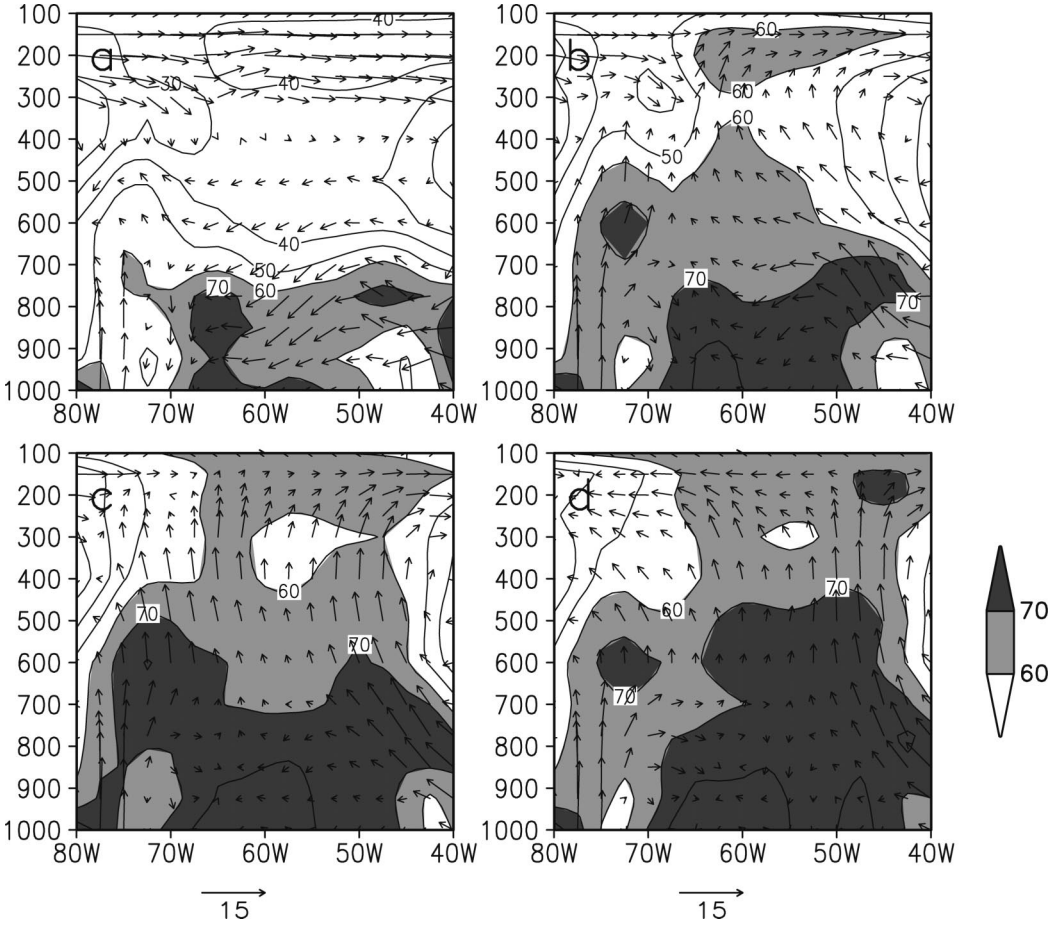

FIG. 11. Pressure–longitude cross section of the composites of zonal and vertical velocity (m s^{-1}, vectors; here, vertical wind is enlarged by 10 times for clarity) and relative humidity (shaded area and contour) along 10°S at (a) pentad −16, (b) pentad −6, (c) pentad 0, and (d) pentad 6, respectively.

gent to rotational kinetic energy conversion. The 200-hPa geopotential height is as low as that in the dry season (Fig. 7). The lack of changes in the large-scale circulation further confirms that the destabilization of the atmosphere during the initiating phase is mainly caused by the increase of the surface latent heat flux and, consequently, humidity in the lower troposphere. The beginning of rainfall increase and the transition from net moisture divergence to convergence (shown in Figs. 6b,c) are probably driven by the increase of the surface latent heat flux and the humidity, instead of by changes of large-scale circulation. The important impact of moisture increase in the lower troposphere on the change of convective instability and on the change of precipitation type from the dry to wet seasons is also suggested by radiosonde observations (Fu et al. 1999) and is consistent with the findings of Petersen and Rutledge (2001).

b. Developing phase (pentads −9 to 0)

The developing phase is marked by the increasing importance of the dynamic process and the acceleration of the transition. It begins with reversals of both the V index and the sign of the energy conversion function, and it ends at the onset of the rainy season with the diminishing of positive $\partial\theta_e/\partial t$ at 850 hPa thereafter. CAPE increases from 0.7 to about 1 kJ kg^{-1} and CINE decreases from 0.07 to 0.04 kJ kg^{-1} at this stage (Fig. 10). The V index has changed from southerly to northerly. The northerly cross-equatorial flow brings moist air from the Caribbean Sea to the Amazon basin (Wang and Fu 2002) and consequently changes the net moisture flux from divergence to convergence (Fig. 6c). As expected from the blocking by the Andes of the prevailing easterly wind, Fig. 8c shows that the zonal moisture flux converges to the region throughout all seasons. This may help to maintain a relatively humid dry season over the southern Amazon region. However, the net moisture divergence is near zero because the zonal convergence is compensated by the meridional divergence before the wet-season onset. The seasonal change of the net large-scale moisture divergence is mainly controlled by the cross-equatorial moisture flux (Fig. 8c).

During this stage of the transition, the rate of increase of evapotranspiration remains about the same as that in the initiating stage (Fig. 8b), but the net moisture convergence soon becomes a significant source of water vapor. The total water vapor gain within the domain increases by 50% compared to the initiating phase, and the relative humidity near the surface increases to 80% (Fig. 11b). Precipitation during the developing phase increases steadily but is still below the threshold for the wet-season onset (Fig. 6e).

Rising motion appears about 45 days before the onset (pentads −9 to −6) over the southern Amazon region and becomes stronger with time (Fig. 11). The middle troposphere becomes more humid (RH $\geq$ 50%), presumably due to more frequent occurrence of deep convection. The composite streamlines at 200 hPa in Fig. 12 show that anticyclonic circulation in the upper atmosphere begins to form to the southwest of the Amazon basin at pentad −6. It becomes stronger and moves southward with the Amazon convection. These changes are consistent with the expected upper-tropospheric response to the increasing convection over the Amazon (Lenters and Cook 1997). Geopotential height at 200 hPa also increases about 60 m (about 2/3 of the total increase from the dry to the wet seasons) within the 30 days prior to the onset of the wet season (Fig. 7), suggesting a rapid stretching of the tropospheric column.

The aforementioned developments in $\partial\theta_e/\partial t$ at 850 hPa, the vertical motion, rainfall, and the 200-hPa geopotential height are consistent with the energetics of the atmospheric circulation during the transition. The increase of $\partial\theta_e/\partial t$ at 850 hPa during both initiating and developing phases indicates an increase of the moist static energy in the lower troposphere (Fig. 6a). The moderate increase of rain rate (about 1 mm day^{-1}) at the beginning of the developing phase suggests a beginning of the stretching of the tropospheric column, which transforms moist static energy to divergent kinetic energy (Moscati and Rao 2001). The conversion function becomes positive (Fig. 6d) about 50 days prior to this onset (pentad −10) and increases steadily to its maximum at the onset of the wet season (pentad 0). This suggests the transformation of divergent kinetic energy into rotational kinetic energy. The vertical profiles of the kinetic energy conversion function at different stages of the transition period have been shown in Fig. 13. In contrast to the negative conversion function through most of the troposphere prior to the developing phase, the vertically integrated C becomes positive during the developing phase. The peak of the conversion function is initially near 250 hPa, then becomes stronger and rises to 200 hPa toward the onset (Fig. 13). Hence, the increase of the energy transformation mainly occurs in the upper troposphere centered at 10°–15°S, 55°–70°W, where the anticyclonic circulation is enhanced rapidly during the developing stage (Fig. 12). Evidently, the development of the wet-season circulation pattern over South America is supported by energy conversions similar to those of the south Asian monsoon.

c. Maturing phase (after pentad 0)

In the maturing phase, the increase of surface fluxes weakens with the decrease of downward solar radiation and net radiative flux at the surface (Fig. 9b). The transition appears to be driven by a positive response of moisture convergence to increased rainfall. As shown in Fig. 6a, the increase of $\partial\theta_e/\partial t$ at 850 hPa becomes insignificant. The northerly V index steadily increases to its full strength (Fig. 6b), doubling the magnitude of moisture convergence in the developing stage. Consequently, the moisture convergence becomes a greater

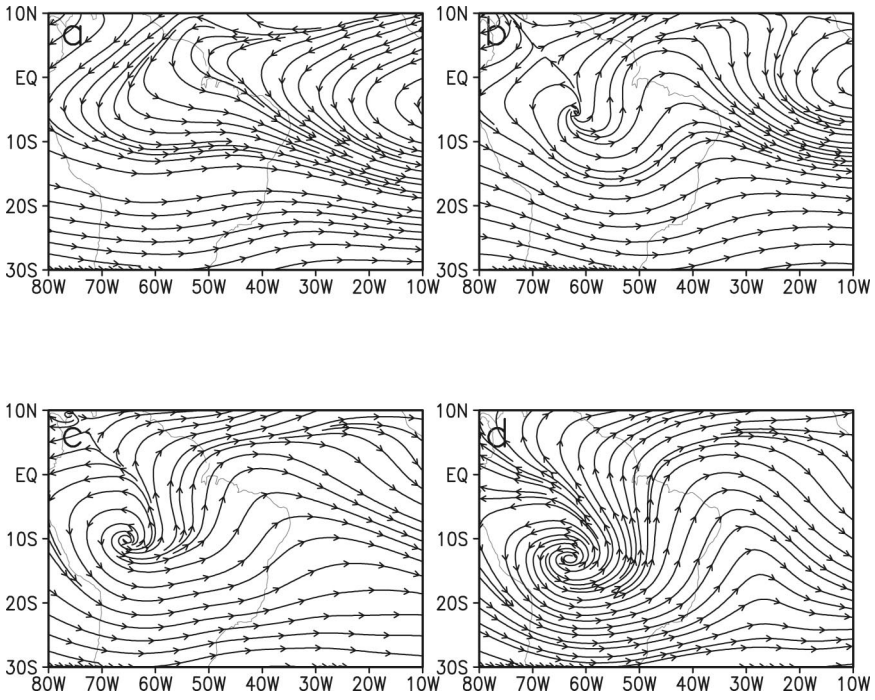

FIG. 12. Composite 200-hPa streamline at (a) pentad −16, (b) pentad −6, (c) pentad 0, and (d) pentad 6, respectively.

source of water vapor than the evapotranspiration (Fig. 8b). Precipitation gradually increases to its annual peak of about 8–9 mm day^{-1} (Fig. 6e).

Figures 11c,d show that the rising motion over the southern Amazon region is maintained at approximately the same strength from the onset. But high RH (≥70%) has penetrated further to 400 hPa, presumably due to the accumulated effect of upward convective transport of water vapor. From pentad 0 to 6, the increase of geopotential height suggests a continuous stretching of the atmospheric column within the 30 days after the onset (Fig. 7). The positive, but much weaker, conversion function (Fig. 6d) indicates a continuous gain of rotational kinetic energy in the upper-tropospheric flow at a much decreased rate. A closed center of upper-tropospheric anticyclonic circulation, associated with the Bolivian high, forms near 18°S about 9–10 pentads (45 days) after the onset of the Amazon wet season (not shown). The results of Figs. 6 and 7 suggest that the convective heating over the Amazon contributes to the development of the Bolivian high, which is consistent with the previous numerical model results of Silva Dias et al. (1983), Gandu and Geisler (1991), and Lenters and Cook (1997).

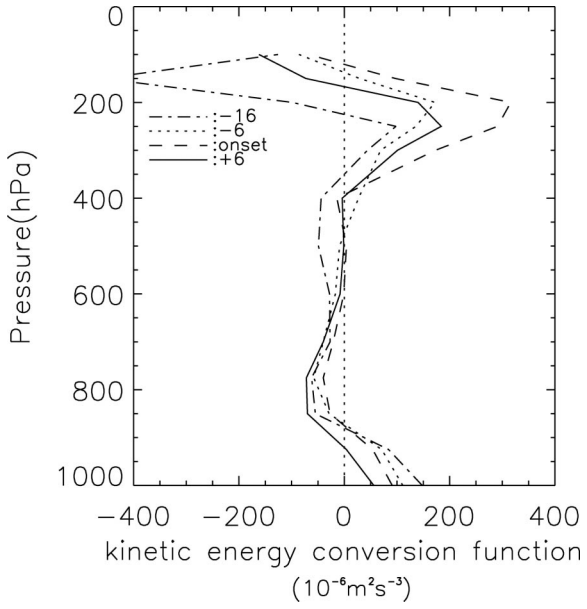

FIG. 13. Vertical profiles of the composite kinetic energy conversion function (10^{-6} m^2 s^{-3}) at pentad −16 (dash–dotted line), pentad −6 (dotted line), pentad 0 (dashed line), and pentad 6 (solid line) averaged over the southern Amazon region.

4. Discussion

a. The role of local land surface processes and large-scale transport

Previous studies have shown that both land surface and large-scale dynamic processes influence the Amazon rainfall. However, their relative importance at different stages of the transition, and therefore the influences of land surface change and climate variability of oceans on the Amazon rainfall, has been unclear. Our

analyses indicate that the increases in surface fluxes, especially latent heat flux, responding to the increase of net radiation on the surface are the dominant contributors to the increase of potential energy and water vapor during the initiating phase of the transition. Thus, land surface processes should have the most significant impact during the initiating phase and should become less crucial during the developing and maturing stages. A drier land surface during the dry season, either caused by a reduced rainfall or by an increase of runoff due to land use, could slow the buildup of the local moist static energy and consequently delay the transition of the large-scale circulation and wet-season onset. The large-scale circulation change associated with SST anomalies in the adjacent oceans could affect the onset at all stages, perhaps being most effective during the developing phase of the onset. During this phase, atmospheric transport becomes an important source of moisture, a deep layer of static instability is needed for convective breakthrough, and favorable upper-tropospheric circulation is needed to reinforce the lower-tropospheric convergence. The changes of the large-scale circulation can easily influence these key factors of the transition from the dry to wet seasons.

b. Similarities and differences between the South American and south Asian monsoons

South America has not been considered a monsoon region because the climatological wind reversal from summer to winter was unclear (e.g., Ramage 1971; Ayoade 1983). However, Zhou and Lau (1998) demonstrate that the patterns of seasonal change for the atmospheric circulation over South America are similar to those of a monsoon system when annual means are removed. Our analyses further suggest that the reversal of the cross-equatorial meridional flow and transport of moisture, the sources and transformation of energy, as well as the evolution of the 200-hPa geopotential height over South America, are similar to those of the south Asian monsoon. However, the South American system differs in several features: the increase of land surface latent heat flux can increase rainfall, which presumably contributes to the reversal of the cross-equatorial flow and moisture convergence; and the relatively high surface latent heat flux and zonal moisture convergence can maintain a relatively humid dry season. Because of the impact of surface latent heat flux on the moist static energy, the development of a continental-scale thermal low due to the increase of sensible heat flux, as in the classic monsoon onset process (Kawamura et al. 2002), is not dominant over South America. The above differences are consistent with the contrasts in geographic location, topography, and land surface type between South America and south Asia. These contrasts include the following:

1) THE WEAKER DIFFERENTIAL HEATING BETWEEN THE CONTINENT AND ADJACENT OCEANS

The Altiplano Plateau is about 1/12 the horizontal area and 1/2 the altitude of the Tibetan Plateau, although the sensible heat flux at the surface appears to be comparable between the two regions (Rao and Erdogan 1989). The tropical location of the Amazon basin, representing the bulk of the South American landmass, leads to a warmer and more humid winter climate compared to that of the subtropical Indian subcontinent, and a weaker and less effective differential heating occurs between the continent and the adjacent ocean. The strong contrast (as much as 5°C) between the SSTs of the eastern Pacific cold tongue and the land surface temperatures of the South American continent (Oliver and Fairbridge 1987) only weakly links these two regions (e.g., Grimm and Silva Dias 1995; Fu et al. 2001) because the Andes blocks the low-level flow between them. Conversely, the atmosphere is significantly more humid and less stable during the dry season in tropical South America than in south Asia, so that its transition can be initiated by relatively small variations of land surface conditions.

2) THE GREATER IMPORTANCE OF HUMIDITY

Radiosonde observations have shown that even during the dry season, the atmosphere over the Amazon is almost statically neutral. The main thermodynamic change from the dry to wet seasons is from the increasing humidity (Fu et al. 1999; Betts and Jakob 2002). Over the Amazon, the prevailing easterly wind transports warm and humid air from the equatorial Atlantic (Satyamurty et al. 1998). Hence, convective instability can be reached with relatively small increases in humidity. Numerical experiments demonstrated that the direct mechanical and sensible heating effects of the Andes on the origin of the Bolivian high are secondary compared to the precipitation over the Amazon basin, central Andes, and South Atlantic convergence zone (Kleeman 1989; Lenters and Cook 1997). In contrast, the formation of the Tibetan high, driven primarily by sensible heat flux (e.g., Li and Yanai 1996), and the reversal of the low-level flow are needed to initiate the increase in precipitation over south Asia.

c. Possible prediction factors

Our analysis may help to identify the potential precursors for onset of the wet season over tropical South America. For short-term prediction of onset (5–10 days), a 20% or more increase of RH, a persistent increase of the northerly pentad V index to 1 m s^{-1} or higher, a persistent decrease of CINE to 40 J kg^{-1}, and the formation of an anticyclonic center at 10°S, together with rain rate, are likely to indicate the onset of the rainy season. For medium-term (2–3 months) prediction, a

delayed or weak increase of the surface fluxes in later austral winter, a delayed reversal of the V index or a weak northerly V index (Wang and Fu 2002), and abnormally strong upper-tropospheric westerlies in early spring probably indicate a delay of the rainy-season onset. The latter, in turn, could delay the development of the Bolivian high in the subtropical South American region. These potential prediction factors are applicable only on a large scale. Their use as quantitative criteria for the wet-season onset still needs to be further explored. The precise date of the onset varies geographically within the Amazon. The link between the large-scale circulation change and the local onset also needs to be further studied.

5. Summary and conclusions

We have applied composite analyses of the changes of land surface and atmospheric variables at pentad (5 day) resolution during the transition from the dry to wet seasons over the southern Amazon basin (5°–15°S, 45°–75°W), using 15-yr instantaneous ERA data (1979–93) and ANEEL rain gauge and GPCP data. The results suggest that the transition is initiated by an increase of local land surface fluxes and then accelerated by dynamic responses to the increase of potential energy in the lower troposphere. The transition can be divided into three stages according to changes in the main driving process. The initiating stage ranges from 90 to 50 days before the onset of the rainy season. This stage is dominated by an increase of equivalent potential temperature in the lower troposphere. This is caused by increasing land surface fluxes, especially the latent heat flux, which consequently reduce CINE and increase the buoyancy and the available potential energy of the lower troposphere. Rain rate also begins to increase. The cross-equatorial flow and upper-tropospheric circulation during this stage remain unchanged from those of the dry season. The developing stage starts with the reversal of cross-equatorial flow in the western Amazon from southerly (during the dry season) to northerly about 45 days before onset. This wind reversal increases moisture transport from the Caribbean Sea; therefore, the transport supplies as much moisture as the evapotranspiration. Increasing moisture transport doubles the total moisture gain over the southern Amazon region, compared to the initiating phase. The latter increases the frequency of convection and consequently increases geopotential height at 200 hPa.

In the upper troposphere, the positive energy conversion function suggests that divergent kinetic energy resulting from the stretching of the atmosphere column is transformed into rotational kinetic energy and consequently spins up the anticyclonic circulation. The stretching effect also reinforces the low-level convergence. This positive feedback accelerates the establishment of a circulation pattern favorable for the onset of the wet season. The maturing stage begins with the onset of the Amazon rainy season and lasts about 30–60 days after the onset, when precipitation and the 200-hPa geopotential height peak. Presumably due to an increase of cloudiness, which reduces the surface solar radiation, the increase of lower-level potential energy is dissipated. The increase of rainfall and further development of the wet-season circulation pattern appear to be dominated by a positive feedback between the upper-level atmospheric anticyclonic circulation and the lower-tropospheric convergence. The South American monsoon circulation matures during this phase.

Our findings help clarify the apparent discrepancy in the literature regarding the relative importance of surface evapotranspiration and large-scale moisture transport in determining the onset of the wet season. Our results suggest that the increase of surface evapotranspiration and local water recycling are key for initiating the transition from the dry to wet seasons. At the developing and mature phases, water fluxes and the large-scale moisture transport to the Amazon both become important. Hence, if the increase of surface evapotranspiration is significantly weakened during the initiating phase, for example, by an increase of runoff due to land use or a decrease of rainfall in previous seasons, the onset of the wet season would probably be delayed. The changes in the large-scale circulation, such as those due to SST changes in the adjacent tropical Pacific and Atlantic, could directly influence the developing and maturing phases of the transition through their control over weakening of the moisture transport or the transition of upper-tropospheric circulation. They can also indirectly influence the surface fluxes through their control of rainfall and cloudiness during dry seasons and the initiating phase of transitions.

Our findings also suggest that the development of the South American monsoon has dynamic and energetic processes similar to those of the classic south Asian monsoon. Especially similar are the dependence of onset on the reversal of the cross-equatorial flow and the conversion of potential energy to divergent kinetic energy and then to rotational kinetic energy. Conversely, the increase of the surface latent heat flux plays a more important role than the increase of the surface sensible heat flux in initiating the wet-season onset over the southern Amazon region. The increase of rainfall and moisture in the lower troposphere begins even before the reversal of the cross-equatorial flow. Thus, early increase of rainfall enables a quicker reversal of the large-scale circulation (Rind and Rossow 1984) than that of the Asian monsoon, which is mainly initiated by the increase of the sensible heat flux.

The validity of the mechanisms suggested by this study can be tested by examining the interannual variations of the wet-season onset, especially in terms of the changes of one or more key factors identified in this study as contributing to the observed early or later onsets. This will be the focus of our future investigations.

Due to a lack of adequate observations, our results

are derived from ERA. While ERA data probably qualitatively capture most of the important features of the seasonal transition over the southern Amazon region, further validation of our results is clearly needed when more adequate observations become available.

Acknowledgments. This work was supported by the NOAA/PACS project. We thank Dr. Brent Liebmann and Mr. Dave Allured for kindly sharing the rain gauge data over tropical South America with us, Drs. Hui Wang and Robert E. Dickinson for constructive discussions, two anonymous reviewers for their insightful comments, and Margaret Sanderson Rae for her editorial assistance.

REFERENCES

Aceituno, P., 1988: On the functioning of the Southern Oscillation in the South American sector. Part I: Surface climate. *Mon. Wea. Rev.,* **116,** 505–524.

Ayoade, J. O., 1983: *Introduction to Climatology for the Tropics.* Vail-Ballou Press Inc., 258 pp.

Betts, A. K., and C. Jakob, 2002: Evaluation of the diurnal cycle of precipitation, surface thermodynamics, and surface fluxes in the ECMWF model using LBA data. *J. Geophys. Res.,* **107,** 8045, doi:10.1029/2001JD000427.

Chu, P. S., 1985: A contribution of the upper-air climatology of tropical South America. *J. Climatol.,* **5,** 403–416.

Covey, D. L., and S. Hastenrath, 1978: The Pacific El Niño phenomenon and the Atlantic circulation. *Mon. Wea. Rev.,* **106,** 1280–1287.

Fu, R., B. Zhu, and R. E. Dickinson, 1999: How do atmosphere and land surface influence seasonal changes of convection in the tropical Amazon? *J. Climate,* **12,** 1306–1321.

——, R. E. Dickinson, M. Chen, and H. Wang, 2001: How do tropical sea surface temperatures influence the seasonal distribution of precipitation in the equatorial Amazon? *J. Climate,* **14,** 4003–4026.

Gandu, A. W., and J. E. Geisler, 1991: A primitive equations model study of the effect of topography on the summer circulation over tropical South America. *J. Atmos. Sci.,* **48,** 1822–1836.

Gibbs, J. R., 1979: Mechanism controlling world water chemistry. *Science,* **170,** 1088–1090.

Gill, A. E., 1980: Some simple solutions for heat-induced tropical circulation. *Quart. J. Roy. Meteor. Soc.,* **106,** 447–462.

Grimm, A. M., and P. L. Silva Dias, 1995: Analysis of tropical–extratropical interactions with influence functions of a barotropic model. *J. Atmos. Sci.,* **52,** 3538–3555.

Gutman, G. J., and W. Schwerdtfeger, 1965: The role of latent and sensible heat for the development of a high-pressure system over the subtropical Andes in the summer. *Meteor. Rundsch.,* **18,** 69–76.

Hastenrath, S., 1990: The relationship of highly reflective clouds to tropical climate anomalies. *J. Climate,* **3,** 353–365.

——, and L. Heller, 1977: Dynamics of climatic hazards in northeast Brazil. *Quart. J. Roy. Meteor. Soc.,* **103,** 77–92.

Horel, J. D., A. N. Hahmann, and J. E. Geisler, 1989: An investigation of the annual cycle of convective activity over the tropical Americas. *J. Climate,* **2,** 1388–1403.

Kawamura, R., Y. Fukuta, H. Ueda, T. Matsuura, and S. Lizuka, 2002: A mechanism of the onset of the Australian summer monsoon. *J. Geophys. Res.,* **107,** 4204, doi:10.1029/2001JD001070.

Kleeman, R., 1989: A modeling study of the effect of the Andes on the summertime circulation of tropical South America. *J. Atmos. Sci.,* **46,** 3344–3362.

Kousky, V. E., 1988: Pentad outgoing longwave radiation climatology for the South American sector. *Rev. Bras. Meteor.,* **3,** 217–231.

Krishnamurti, T. N., and Y. Ramanathan, 1982: Sensitivity of the monsoon onset to differential heating. *J. Atmos. Sci.,* **39,** 1290–1306.

——, M. C. Sinha, B. Jha, and U. C. Mohanty, 1998: A study of south Asian monsoon energetics. *J. Atmos. Sci.,* **55,** 2530–2548.

Lenters, J. D., and K. H. Cook, 1997: On the origin of the Bolivian high and related circulation features of the South American climate. *J. Atmos. Sci.,* **54,** 656–678.

Li, C., and M. Yanai, 1996: The onset and interannual variability of the Asian summer monsoon in relation to land–sea thermal contrast. *J. Climate,* **9,** 358–375.

Liebmann, B., and J. A. Marengo, 2001: Interannual variability of the rainy season and rainfall in the Brazilian Amazon basin. *J. Climate,* **14,** 4308–4318.

Marengo, J. A., B. Liebmann, V. E. Kousky, N. P. Filizola, and I. C. Wainer, 2001: Onset and end of the rainy season in the Brazilian Amazon basin. *J. Climate,* **14,** 833–852.

Markham, C. G., and D. R. McLain, 1977: Sea surface temperature related to rain in Ceará, northeastern Brazil. *Nature,* **265,** 320–323.

Moscati, M. C. D., and V. B. Rao, 2001: Energetics of the summer circulation over South America. *Ann. Geophys.,* **19,** 83–97.

Moura, A. D., and J. Shukla, 1981: On the dynamics of droughts in northeast Brazil: Observations, theory, and numerical experiments with a general circulation model. *J. Atmos. Sci.,* **38,** 2653–2675.

Namias, J., 1972: Influence of Northern Hemisphere general circulation on drought in northeast Brazil. *Tellus,* **24,** 336–342.

Nishizawa, T., and M. Tanaka, 1983: The annual change in the tropospheric circulation and the rainfall in South America. *Arch. Meteor. Geophys. Bioklmatol.,* **33,** 107–116.

Oliver, J. E., and R. W. Fairbridge, 1987: *The Encyclopedia of Climatology.* Van Nostrand Reinhold, 986 pp.

Petersen, W., and S. A. Rutledge, 2001: Regional variability in tropical convection: Observations from TRMM. *J. Climate,* **14,** 3566–3586.

Ramage, C. S., 1971: *Monsoon Meteorology.* Academic Press, 296 pp.

Rao, G. V., and S. Erdogan, 1989: The atmospheric heat source over the Bolivian plateau for a mean January. *Bound-Layer Meteor.,* **46,** 13–33.

Rao, V. B., I. F. A. Cavalcanti, and K. Hada, 1996: Annual variation of rainfall over Brazil and water vapor characteristics over South America. *J. Geophys. Res.,* **101,** 26 539–26 551.

Rind, D., and W. B. Rossow, 1984: The effects of physical processes on the Hadley circulation. *J. Atmos. Sci.,* **41,** 479–507.

Ropelewski, C. F., and M. S. Halpert, 1989: Precipitation patterns associated with the high index phase of the Southern Oscillation. *J. Climate,* **2,** 268–284.

Rowntree, P. R., 1976: Response of the atmosphere to a tropical Atlantic Ocean temperature anomaly. *Quart. J. Roy. Meteor. Soc.,* **102,** 607–625.

Salati, E., A. Dall'Olio, J. Gat, and E. Matsui, 1979: Recycling of water in the Amazon basin: An isotope study. *Water Resour. Res.,* **15,** 1250–1258.

Satyamurty, P., C. A. Nobre, and P. L. Silva Dias, 1998: South America. *Meteorology of the Southern Hemisphere, Meteor. Monogr.,* No. 49, Amer. Meteor. Soc., 119–139.

Serra, A., 1973: Statistical aspects of northeast Brazil droughts. *Bol. Geogr. Rio de Janeiro,* **32** (233) 1–153.

Silva Dias, P. L., W. H. Schubert, and M. DeMaria, 1983: Large-scale response of the tropical atmosphere to transient convection. *J. Atmos. Sci.,* **40,** 2689–2707.

Virji, H., 1981: A preliminary study of summertime tropospheric circulation patterns over South America estimated from cloud winds. *Mon. Wea. Rev.,* **109,** 599–610.

Wang, H., and R. Fu, 2002: Cross-equatorial flow and seasonal cycle of precipitation over South America. *J. Climate,* **15,** 1591–1608.

Williams, E., and N. Renno, 1993: An analysis of the conditional instability of the tropical atmosphere. *Mon. Wea. Rev.,* **121,** 21–36.

Zhou, J. Y., and K.-M. Lau, 1998: Does a monsoon climate exist over South America? *J. Climate,* **11,** 1020–1040.